Article

Membrane Dynamics of the Amphiphilic Siderophore, Acinetoferrin

Minkui Luo, Evgeny A. Fadeev, and John T. Groves

J. Am. Chem. Soc., **2005**, 127 (6), 1726-1736• DOI: 10.1021/ja044230f • Publication Date (Web): 25 January 2005

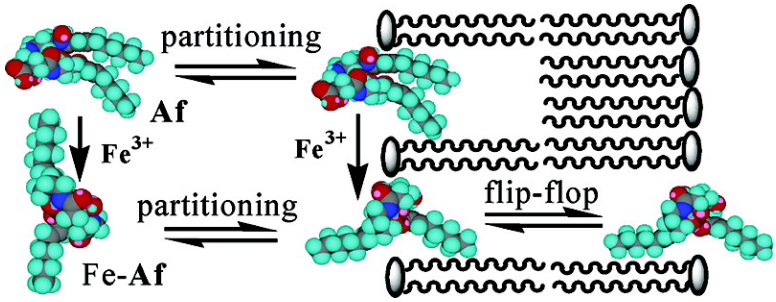

More About This Article

Additional resources and features associated with this article are available within the HTML version:

- Supporting Information
- Links to the 1 articles that cite this article, as of the time of this article download
- Access to high resolution figures
- Links to articles and content related to this article
- Copyright permission to reproduce figures and/or text from this article

View the Full Text HTML

J|A|C|S
ARTICLES
Published on Web 01/25/2005

Membrane Dynamics of the Amphiphilic Siderophore, Acinetoferrin

Minkui Luo, Evgeny A. Fadeev, and John T. Groves*

Contribution from the Department of Chemistry, Princeton University, Princeton, New Jersey 08540

Received September 22, 2004; E-mail: jtgroves@princeton.edu

Abstract: *Acinetobacter haemolyticus* is an antibiotic resistant, pathogenic bacterium responsible for an increasing number of hospital infections. Acinetoferrin (**Af**), the amphiphilic siderophore isolated from this organism, contains two unusual *trans*-2-octenoyl hydrocarbon chains reminiscent of a phospholipid structural motif. Here, we have investigated the membrane affinity of **Af** and its iron complex, Fe−**Af**, using small and large unilamellar phospholipid vesicles (SUV and LUV) as model membranes. **Af** shows a high membrane affinity with a partition coefficient, $K_x = 6.8 \times 10^5$. Membrane partitioning and trans-membrane flip-flop of Fe−**Af** have also been studied via fluorescence quenching of specifically labeled vesicle leaflets and ^{1}H NMR line-broadening techniques. Fe−**Af** is found to rapidly redistribute between lipid and aqueous phases with dissociation/partitioning rates of $k_{off} = 29\ s^{-1}$ and $k_{on} = 2.4 \times 10^4\ M^{-1}\ s^{-1}$, respectively. Upon binding iron, the membrane affinity of **Af** is reduced 30-fold to $K_x' = 2.2 \times 10^4$ for Fe−**Af**. In addition, trans-membrane flip-flop of Fe−**Af** occurs with a rate constant, $k_p = 1.2 \times 10^{-3}\ s^{-1}$, with egg-PC LUV and a half-life time around 10 min with DMPC SUV. These properties are due to the phospholipid-like conformation of **Af** and the more extended conformation of Fe−**Af** that is enforced by iron binding. Remarkable similarities and differences between **Af** and another amphiphilic siderophore, marinobactin E, are discussed. The potential biological implications of **Af** and Fe−**Af** are also addressed. Our approaches using *inner*- and *outer*-leaflet-labeled fluorescent vesicles and ^{1}H NMR line-broadening techniques to discern **Af**-mediated membrane partitioning and trans-membrane diffusion are amenable to similar studies for other paramagnetic amphiphiles.

Introduction

Although iron is one of the most abundant elements on earth, its microbial bioavailability is limited due to the extremely low solubility of iron(III) oxides under aqueous aerobic conditions.[1,2] To surmount this problem, most bacteria secrete siderophores, small organic molecules with a high affinity for iron(III).[3,4] Among the hundreds of known siderophores, there is a small subfamily of *amphiphilic* siderophores that typically contain a hydrophilic iron-binding headgroup and one or two hydrophobic side chains. The first amphiphilic siderophores to be identified were the mycobactins.[5] Several classes of amphiphilic siderophores have been isolated from a large number of terrestrial bacteria.[6−11] It was recently reported that marine microorganisms also adopt similar siderophore-mediated strategy to overcome iron deficiency in the oceans.[12] Three suites of amphiphilic siderophores, marinobactins, aquachelins, and amphibactins, with lipopeptide-like structures were characterized from different oceanic strains.[12,14] Thus, it is apparent that amphiphilic siderophores play important biological roles in bacterial iron-acquisition in a variety of iron-deficient circumstances.

Acinetoferrin (**Af** as indicated in Figure 1) is a citrate-based amphiphilic siderophore produced by *Acinetobacter haemolyticus*,[7] the most prevalent proteolytic species of the ubiquitous

(1) Albrecht-Gary, A. M.; Crumbliss, A. L. *Met. Ions Biol. Syst.* **1998**, *35*, 239−327.
(2) Boukhalfa, H.; Crumbliss, A. L. *Biometals* **2002**, *15*, 325−339.
(3) (a) Ratledge, C.; Dover, L. G. *Annu. Rev. Microbiol.* **2000**, *54*, 881−941. (b) Raymond, K. N.; Dertz, E. A.; Kim, S. S. *Proc. Natl. Acad. Sci. U.S.A.* **2003**, *100*, 3584−3588. (c) Bluhm, M. E.; Kim, S. S.; Dertz, E. A.; Raymond, K. N. *J. Am. Chem. Soc.* **2002**, *124*, 2436−2437.
(4) (a) Roosenberg, J. M.; Lin, Y. M.; Lu, Y.; Miller, M. J. *Curr. Med. Chem.* **2000**, *7*, 159−197. (b) Bergeron, R. J.; McManis, J. S.; Franklin, A. M.; Yao, H.; Weimar, W. R. *J. Med. Chem.* **2003**, *46*, 5478−5483. (c) Bergeron, R. J.; Wiegand, J.; McManis, J. S.; Bussenius, J.; Smith, R. E.; Weimar, W. R. *J. Med. Chem.* **2003**, *46*, 1470−1477. (d) Bergeron, R. J.; McManis, J. S.; Bussenius, J.; Brittenham, G. N.; Wiegand, J. *J. Med. Chem.* **1999**, *42*, 2881−2886.
(5) Francis, J.; Macturk, H. M.; Madinaveitia, J.; Snow, G. A. *Biochem. J.* **1953**, *55*, 596−607.
(6) Lynch, D.; O'Brien, J.; Welch, T.; Clarke, P.; Cuiv, P. O.; Crosa, J. H.; O'Connell, M. *J. Bacteriol.* **2001**, *183*, 2576−2585.
(7) Okujo, N.; Sakakibara, Y.; Yoshida, T.; Yamamoto, S. *Biometals* **1994**, *7*, 170−176.
(8) Persmark, M.; Pittman, P.; Buyer, J. S.; Schwyn, B.; Gill, P. R.; Neilands, J. B. *J. Am. Chem. Soc.* **1993**, *115*, 3950−3956.
(9) Risse, D.; Beiderbeck, H.; Taraz, K.; Budzikiewicz, H.; Gustine, D. *Z. Naturforsch., C: Biosci.* **1998**, *53*, 295−304.
(10) (a) Stephan, H.; Freund, S.; Beck, W.; Jung, G.; Meyer, J. M.; Winkelmann, G. *Biometals* **1993**, *6*, 93−100. (b) Stephan, H.; Freund, S.; Meyer, J. M.; Winkelmann, G.; Jung, G. *Liebigs Ann. Chem.* **1993**, 43−48.
(11) Groves, J. T. *Proc. Natl. Acad. Sci. U.S.A.* **2003**, *100*, 3569−3574.
(12) (a) Martinez, J. S.; Carter-Franklin, J. N.; Mann, E. L.; Martin, J. D.; Haygood, M. G.; Butler, A. *Proc. Natl. Acad. Sci. U.S.A.* **2003**, *100*, 3754−3759. (b) Martinez, J. S.; Zhang, G. P.; Holt, P. D.; Jung, H. T.; Carrano, C. J.; Haygood, M. G.; Butler, A. *Science* **2000**, *287*, 1245−1247.
(13) Levitt, M. H. *Spin Dynamics: Basics of the Nuclear Magnetic Resonance*; John Wiley & Sons: Chichester, New York, Weinheim, Brisbane, Singapore, Toronto, 2001.
(14) (a) Xu, G. F.; Martinez, J. S.; Groves, J. T.; Butler, A. *J. Am. Chem. Soc.* **2002**, *124*, 13 408−13 415. (b) Xu, G. F. Synthesis and Analyses of Materials at Interfaces: From Organic Soft Materials to Inorganic Hard Materials. Ph.D. Thesis, the Department of Chemistry, Princeton University, 2002, Chapter 8.

10.1021/ja044230f CCC: $30.25

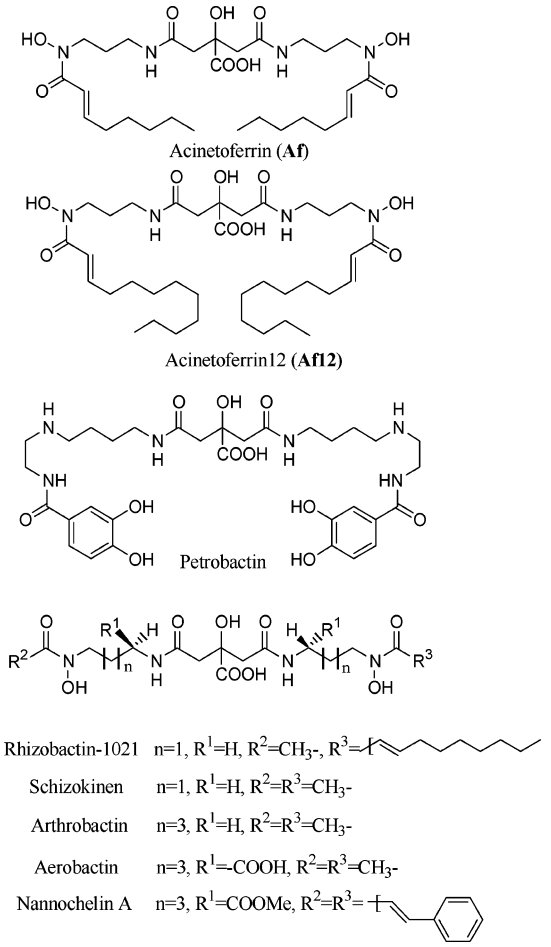

Figure 1. Structures of citrate-based siderophores.

Acinetobacter genus.[16] An increasing number of *Acinetobacter*-mediated hospital infections and outbreaks have been reported recently since these organisms are highly resistant to many antibiotics in common use, including β-lactams, macrolides, and quinolones.[7,17,18] **Af** secreted by A*cinetobacter* and its derivative, acinetoferrin imide, is able to cross-feed iron to *Mycobacterium paratuberculosis* and *Mycobacterium tuberculosis*, two pathogenic strains that are responsible for Crohn's disease and lethal tuberculosis in humans, respectively.[19] The emergence of these infections and their corresponding multidrug resistances make it important to understand the **Af**-mediated iron transport. Moreover, accumulated knowledge here will further help the development of new drugs based on siderophores and their drug conjugates.[4,20,21]

The iron-chelating groups of **Af** consist of one α-hydroxy carboxylic acid within its citrate subunit and two hydroxamates appended to aminopropyl skeletal linkers. These chelating and structural features of the citrate subunit in **Af** are also adopted by other citrate-based siderophores (Figure 1), such as schizokinen,[27,28,30,31] rhizobactin-1021,[8] arthrobactin,[27,32] aerobactin,[24,25,29] nannochelin,[23,26] and petrobactin.[22] A novel structural feature of **Af** lies in the two unusual *trans*-2-octenoyl hydrocarbon chains, in contrast to the rest of the known amphiphilic siderophores that only include a single hydrophobic chain.[6−12] The NMR structure of gallium−**Af** that we have recently reported shows that this special arrangement of the two hydrophobic chains in **Af** changes dramatically upon metal binding.[35] Our goal with the current studies was to establish how the molecular structures of **Af** and Fe−**Af** relate to their membrane dynamic properties.

In this work, we describe our studies of the membrane dynamics of acinetoferrin (**Af**) and its iron complex (Fe−**Af**) in phospholipid vesicles as a model membrane. A large difference between the membrane affinities of **Af** and Fe−**Af** is observed with a 30-fold lower partition coefficient for the latter. Fe−**Af** also shows a rapid partitioning/dissociation between the lipid and aqueous phase, with a half-life time in the millisecond scale, and facile membrane permeability through phospholipid bilayers, with a half-life time around 10 min. We interpret these membrane properties to result from the more extended orientation of the two *trans*-2-octenoyl hydrocarbon chains of Fe−**Af**, in contrast to that of **Af**. This unusual construction of the hydrophobic segments in **Af** plays a significant role in its special membrane properties that could be related to the bacterial iron access. The membrane dynamics of amphiphilic siderophores and devising methods to determine them will be important for understanding these aspects of bacterial iron acquisition.

Experimental Section

Reagents and Materials. All reagents were obtained from available commercial sources and used without further purification unless mentioned otherwise. 1,2-Dimyristoyl-*sn*-glycero-3-phosphocholine

(15) In a previous paper,[14] the equation $k_{obs}/k_w = (\alpha - 1)[(K_x \times [\text{vesicle}])/(K_x \times [\text{vesicle}] + [\text{water}])] + 1$ was used instead of eq 2. The additional term $k' \times [\text{vesicle}]$ in eq 2 is to correct for the variation in the ionic strength with varied lipid concentrations. As shown in Figure S3, the relative iron-acquisition rates (k_{obs}/k_w) dropped rapidly after initial addition of lipid vesicles (<2 mM lipid vesicles), and then a slow decrease of k_{obs}/k_w with increased lipid concentrations (from 2 to 15 mM) was observed. We assume that the latter part is due to the variation in the ionic strength with varied lipid concentrations. Therefore, a new term, $k' \times [\text{vesicle}]$, as described in eq 2, was added to correct the slight deviation. By fitting k_{obs}/k_w and lipid concentrations to this equation, a good correlation can still be observed with $k_v/k_w = 0.52$ (the value of α) and $K_x = 3.9 \times 10^5$ for the partition coefficient, consistent with what was obtained by fitting eq 2.

(16) (a) Rudant, E.; Courvalin, P.; Lambert, T. *Antimicrob. Agents Chemother.* **1997**, *41*, 2646−2651. (b) Lambert, T.; Gerbaud, G.; Galimand, M.; Courvalin, P. *Antimicrob. Agents Chemother.* **1993**, *37*, 2093−2100.
(17) Vaneechoutte, M.; Dijkshoorn, L.; Tjernberg, I.; Elaichouni, A.; Devos, P.; Claeys, G.; Verschraegen, G. *J. Clin. Microbiol.* **1995**, *33*, 11−15.
(18) Visalli, M. A.; Jacobs, M. R.; Moore, T. D.; Renzi, F. A.; Appelbaum, P. C. *Antimicrob. Agents Chemother.* **1997**, *41*, 767−770.
(19) (a) Guo, H. Y.; Naser, S. A.; Ghobrial, G.; Phanstiel, O. *J. Med. Chem.* **2002**, *45*, 2056−2063. (b) Dong, L.; Miller, M. J.; Mollmann, U. *Biometals* **2004**, *17*, 99−104. (c) Dhungana, S.; Miller, M. J.; Dong, L.; Ratledge, C.; Crumbliss, A. L. *J. Am. Chem. Soc.* **2003**, *125*, 7654−7663.
(20) Miller, M. J.; Malouin, F. *Acc. Chem. Res.* **1993**, *26*, 241−249.
(21) Lin, Y. M.; Helquist, P.; Miller, M. J. *Synthesis-Stuttgart* **1999**, 1510−1514.
(22) (a) Barbeau, K.; Zhang, G. P.; Live, D. H.; Butler, A. *J. Am. Chem. Soc.* **2002**, *124*, 378−379. (b) Bergeron, R. J.; Huang, G. F.; Smith, R. E.; Bharti, N.; McManis, J. S.; Butler, A. *Tetrahedron* **2003**, *59*, 2007−2014.
(23) Bergeron, R. J.; Phanstiel, O. *J. Org. Chem.* **1992**, *57*, 7140−7143.
(24) Gibson, F.; Magrath, D. I. *Biochim. Biophys. Acta* **1969**, *192*, 175.
(25) Harris, W. R.; Carrano, C. J.; Raymond, K. N. *J. Am. Chem. Soc.* **1979**, *101*, 2722−2727.
(26) Kunze, B.; Trowitzschkienast, W.; Hofle, G.; Reichenbach, H. *J. Antibiot.* **1992**, *45*, 147−150.
(27) Lee, B. H.; Miller, M. J. *J. Org. Chem.* **1983**, *48*, 24−31.
(28) Milewska, M. J.; Chimiak, A.; Glowacki, Z. *J. Prakt. Chem.* **1987**, *329*, 447−456.
(29) Miller, M. J.; Maurer, P. J. *J. Am. Chem. Soc.* **1982**, *104*, 3096−3101.
(30) Mullis, K. B.; Pollack, J. R.; Neilands, J. B. *Biochemistry* **1971**, *10*, 4894.
(31) Plowman, J. E.; Loehr, T. M.; Goldman, S. J.; Sandersloehr, J. *J. Inorg. Biochem.* **1984**, *20*, 183−197.
(32) Schafft, M.; Diekmann, H. *Arch. Microbiol.* **1978**, *117*, 203−207.
(33) We measured surface pressure in the presence of various concentrations of **Af** in the HEPES-buffered solution at pH = 7.4 (100 mM HEPES, 150 mM NaCl). Even if the concentration of **Af** reaches 0.2 mM, there is no obvious indication of the formation of micelles by observing the change of surface pressure vs the concentration of **Af**.
(34) Faller, B.; Nick, H. *J. Am. Chem. Soc.* **1994**, *116*, 3860−3865.
(35) Fadeev, E. A.; Luo, M.; Groves, J. T. *J. Am. Chem. Soc.* **2004**, *126*, 12065−12075.

(DMPC), egg L-α-phosphatidylcholine (egg-PC, 99%), and 1-myristol-2-6-[(7-nitro-2-1,3-benzoxadiazol-4-yl)amino]caproyl-*sn*-glycero-3-phosphocholine (NBD-PC) were purchased from Avanti Polar Lipids, Inc. Anhydrous iron(III) chloride (99.99+%) was purchased from Aldrich. HEPES (sodium salt and free acid) and Tris were purchased from Sigma. All buffered solutions were prepared with 100 mM HEPES and 150 mM NaCl in deionized water unless indicated otherwise. Iron−citrate solution (the molar ratio of iron to citrate is 1:5.7) was prepared as previously described.[34] Acinetoferrin (**Af**) and its analogues were synthesized according to our reported procedures.[35] Stock solutions of acinetoferrin (**Af**, 50 mM) were prepared by dissolving **Af** in DMF/water (volume ratio = 7:10) and stored at −80 °C before use. Stock solutions of Fe−**Af** were produced by premixing **Af** with 1 equiv of iron−citrate and then incubated for 8 h in an aluminum-foil-wrapped flask and freshly used every time.

General Preparation of Vesicles. Unilamellar vesicles were prepared by either sonication for small unilamellar vesicles (SUV) with a diameter of 30−40 nm or membrane extrusion for large unilamellar vesicles (LUV) with a diameter of 200 nm.[14] Briefly, weighed DMPC or egg-PC or egg-PC:cholesterol (1:0.8) was dissolved in chloroform and then transferred into 5 mL test tubes. The thin films of lipid were deposited on the walls of the test tubes after evaporating the solvent with a stream of argon, and then were subjected to high vacuum overnight. The dried lipid films were hydrated in HEPES buffer (100 mM HEPES, 150 mM NaCl) at 40 °C for 30 min. To prepare small unilamellar vesicles (egg-PC or DMPC SUV), the pretreated lipid buffers were sonicated with a probe tip sonicator in an ice−water bath until ice was melted completely, and then the bath temperature reached room temperature (taking about 30 min). To prepare small unilamellar vesicles of egg-PC:cholesterol (1:0.8), the sample was sonicated for 1 h in a 45 °C water bath. After centrifugation of the vesicle suspension at 12 000 r.p.m. for 5 min to remove the sonicator tip debris, a translucent SUV suspension was obtained. To prepare large unilamellar vesicles (LUV), the pretreated lipid buffers were subject to five freeze−thaw cycles by taking turns dipping the test tubes in liquid nitrogen and warm water. The subsequent turbid lipid buffers were extruded 20 times at 40 °C through a polycarbonate membrane with a pore size of 200 nm to yield a translucent LUV suspension. D_2O (30%) in deionized water instead of pure deionized water was used to prepare buffers of DMPC SUV for proton NMR experiments.

Preparation of NBD-PC-Labeled Fluorescent Vesicles. Outer-leaflet-NBD-PC-labeled, double-leaflet-NBD-PC-labeled, and inner-leaflet-NBD-PC-labeled fluorescent vesicles were prepared from NBD-PC fluorescent probe as described previously with some adjustments.[36] Briefly, to prepare outer-leaflet-labeled vesicles, SUV or LUV of DMPC and egg-PC were obtained by sonication or extrusion as described above and then injected into a test tube containing solvent-free NBD-PC (the molar ratio of NBD-PC to DMPC or egg-PC = 1:100). A translucent solution of outer-leaflet-labeled vesicles was formed after a vortex for several seconds and freshly used each time. To yield double-leaflet-labeled vesicles, a 1:100 (molar ratio) mixture of NBD-PC with DMPC (egg-PC) instead of pure DMPC (egg-PC) was subjected to the same procedures described in the previous section of General Preparation of Vesicles. Inner-leaflet-labeled egg-PC vesicles were prepared by a $Na_2S_2O_4$-mediated selective reduction on outer-layer NBD-PC of double-leaflet-labeled vesicles. Briefly, freshly prepared 0.5 mM $Na_2S_2O_4$ (the final concentration) was injected into double-leaflet-labeled egg-PC vesicles (this method does not work for DMPC, see Figure S2 in the Supporting Information). This mixture was subsequently incubated for 1 h at room temperature and then subjected to bubbling dioxygen for 5 min. This additional step of dioxygen-bubbling could better stabilize the inner-leaflet-labeled vesicles by oxidizing excess $Na_2S_2O_4$ and, thereby, create a nonreductive environment for the following membrane-permeability studies of Fe−**Af** (see Figure S2 in the Supporting Information).

(36) McIntyre, J. C.; Sleight, R. G. *Biochemistry* **1991**, *30*, 11819−11827.

UV−Visible Spectroscopy. UV−visible spectroscopy was used to monitor the buildup of Fe−**Af**. Kinetic measurements of the iron-acquisition of **Af** from iron−citrate were performed in HEPES buffer (100 mM HEPES, 150 mM NaCl) at 37 °C by injecting **Af** stock solution into a preincubated iron−citrate solution in the presence of various concentrations of DMPC vesicles (0−15 mM). For all sets of experiments, the final concentrations of **Af** are below the critical micelle concentration (CMC) of **Af**.[33] The absorbance increase of the mixture at 430 nm corresponding to the formation of Fe−**Af** was monitored by a Cary 300 Bio UV−visible spectrophotometer. Experimental data were fit to appropriate kinetic equations using Scientist software.

Measurements of Fluorescence Intensities. Fluorescence intensities of NBD-PC-labeled fluorescent vesicles were measured at room temperature or 37 °C using a Perkin-Elmer LS-50 luminescence spectrometer or Hi-Tech SF-61 DX2 stopped-flow spectrophotometer with a photomultiplier fluorescence mode, respectively. Briefly, for fluorescence measurements at room temperature, outer-leaflet-labeled fluorescent vesicles of various concentrations (0.3−18 mM, final concentration) were mixed with the equal volume of blank buffer or Fe−**Af** stock solutions. The initial intensity, Φ_0, for mixing with blank buffer and quenching intensity, Φ_q, for mixing with Fe−**Af** stock solutions were recorded with the excitation wavelength at 470 nm and the emission wavelength at 540 nm. The relative fluorescence intensities were calculated as $\ln(\Phi_0/\Phi_q)$. Stopped-flow techniques were used to either measure fluorescence intensities at 37 °C or monitor the initial fluorescence decay upon mixing NBD-PC-labeled fluorescent vesicles with Fe−**Af**. One mixing syringe was filled with various concentrations of fluorescent-probe-labeled vesicles. The other one was loaded with Fe−**Af** stock solutions or merely blank buffer. With the excitation wavelength at 460 nm and using a Melles-Griot GG-495 cutoff filter, the variations of fluorescence intensities versus time were recorded upon rapid mixing by cutting off the wavelength below 530 nm. The initial intensity (Φ_0), quenching intensity (Φ_q) at time *t*, and relative intensity ($\ln(\Phi_0/\Phi_q)$) are the same as defined above.

Measurements of Mean Molecular Areas (Mma) Using Langmuir−Blodgett Techniques. Measurements of the mean molecular areas (Mma) of **Af** and its analogues were carried out on a KSV 5000 Langmuir−Blodgett Mini-trough. Substrates (**Af** or its analogues) were dissolved in spectrophotometric grade chloroform and subsequently deposited on the air/subphase interface of Tris buffer (pH = 8.0, 60 mM Tris, 100 mM KCl, and 1 mM $CaCl_2$) or ferric Tris buffer (pH = 8.0, 60 mM Tris, 100 mM KCl, 1 mM $CaCl_2$, and 5 mM ferric ammonium citrate). After incubating for 30 min to allow the evaporation of chloroform, the monolayer surface of an amphiphilic substrate was compressed by moving barrier at a speed of 10 mm/min, and the surface pressure versus mean molecular areas (Mma) was recorded. The headgroup size of the substrate was derived from the value of Mma at zero surface pressure by extrapolating the linear region.

Proton NMR Spectroscopy. The membrane affinity and permeability of Fe−**Af** with DMPC or egg-PC:cholesterol (1:0.8) vesicles as the model membranes were studied using a Varian INOVA 400 MHz proton NMR spectrometer. The ^{1}H NMR line-broadening effects of the choline *N*-methyl groups of DMPC vesicles were monitored as an indicator to detect the partitioning and flip-flop of lipid-phase paramagnetic Fe−**Af**. The evolutions of the two proton resonances at 3.32 and 3.27 ppm, corresponding to the choline *N*-methyl groups of the outer leaflet and the inner leaflet,[14] were recorded after an injection of Fe−**Af** into an NMR tube containing a buffer of 25 mM lipids. Presaturation 1D water suppression was carried out to suppress the proton resonance of water peak.

T_1 relaxation times were measured with the standard inversion−recovery 180-τ-90-acquisition pulse sequence on a Varian Inova 600 MHz proton NMR spectrometer.[13] The experimental parameters were: acquisition time, 4.0 s; relaxation delay, 1.0 s; 99 840 complex data points were collected for each acquisition, and the relaxation recovery of 10 equally spaced intervals between 0.0125 and 2.0 s were used.

The acquired peak maximum intensities for both inner- and outer-layer DMPC SUV choline methyl resonances were fit to a single-exponential decay versus the relaxation delay time. The experimental parameters were chosen so that the T_1 determination experiments were completed within 1 min. Kinetic T_1 measurements were performed by running an array of T_1 experiments spaced by the preset reacquisition delay.

Results

Aqueous-Phase Iron Acquisition from Iron−Citrate Clusters. The kinetics of aqueous-phase iron acquisition by **Af** from iron−citrate clusters were studied using UV−visible spectroscopy. After mixing **Af** with 1 equiv of iron−citrate, an increase of the absorbance at 430 nm was observed, corresponding to the buildup of Fe−**Af** species. The absorbance change at 430 nm displayed double exponential kinetics that fit well to eq 1 (Figure S3, Supporting Information):

$$A_t = A_{pm}[1 - \exp(-k_{pm} \times t)] + A_m[1 - \exp(-k_m \times t)] + C \quad (1)$$

where k_{pm} and k_m correspond to the iron-acquisition rate constants from polymeric and monomeric iron−citrate species, respectively.[34] A_t is the absorbance variation at 430 nm; t is the reaction time (min); A_{pm} and A_m are the absorbance changes resulting from polymeric and monomeric iron−citrate, respectively, and C is the initial fast absorbance jump observed upon mixing. The observed first-order iron-acquisition rate constant from polymeric iron−citrate, $k_{pm} = 5.48 \times 10^{-4}$ s^{-1}, is consistent with an initial conversion of polymeric iron−citrate to a more reactive intermediate.[34,37]

Lipid-Phase Iron Acquisition of Af and Determination of its Partition Coefficient. One important property of amphiphilic molecules is their ability to partition between lipid and aqueous phase. Scheme 1 describes the iron-acquisition pathways of amphiphilic **Af** in the presence of lipid vesicles. The buildup rate, k_{obs}, of Fe−**Af** is assumed to consist of the processes of both aqueous-phase **Af** (k_w) and lipid-vesicle-phase **Af** (k_v), whereas the concentrations of lipid vesicles and the partition coefficient account for the distribution of **Af** between lipid and aqueous phase.[14] The rates of iron removal (k_{obs}) from iron−citrate to **Af** in the presence of various concentrations of DMPC SUV were obtained by measuring absorbance changes at 430 nm and then fitting the data with k_{pm} in eq 1. The relative iron-acquisition rate, k_{obs}/k_w, was calculated by assuming $k_w = k_{pm} = 5.48 \times 10^{-4}$ s^{-1} from Figure S3 for the series of experiments. Because the iron-acquisition rate of **Af** in the aqueous phase (k_w) is not equal to that in the lipid phase, k_v, a hyperbolic relationship between the relative iron-acquisition rate (k_{obs}/k_w) and the lipid-vesicle concentration [vesicle] can be predicted as eq 2, as we have previously described.[14,15]

$$\frac{k_{obs}}{k_w} = (\alpha - 1)\frac{K_x \times [\text{vesicle}]}{K_x \times [\text{vesicle}] + [\text{water}]} + 1 + k' \times [\text{vesicle}] \quad (2)$$

Here, k_{obs}/k_w is the relative iron-acquisition rate as described above; α is defined as k_v/k_w, the ratio of iron-acquisition rate in lipid phase to that in aqueous phase; K_x is the molar fraction partition coefficient of **Af** between vesicle and aqueous phase; [water] and [vesicle] are molar concentrations of water and lipid vesicles, respectively. The term in eq 2, $k' \times$ [vesicle], is to offset the small decrease of k_{obs}/k_w with the increased lipid concentrations in the range from 2 to 15 mM, which we assume is due to the variation of ionic strength with varied lipid concentrations.[15] Figure 2 shows the relationship between the relative iron-acquisition rates, k_{obs}/k_w (filled dots in Figure 2), and increased concentrations of lipid vesicles. After fitting eq 2 to the experimental data, an excellent correlation was obtained (the solid line in Figure 2) with the lipid and aqueous-phase

Scheme 1. Systematic Description on the Membrane Affinity of **Af** (apo- and ferric species) and **Af**-Mediated Iron-Acquisition from Iron−Citrate in Both Aqueous Phase and Lipid Phase

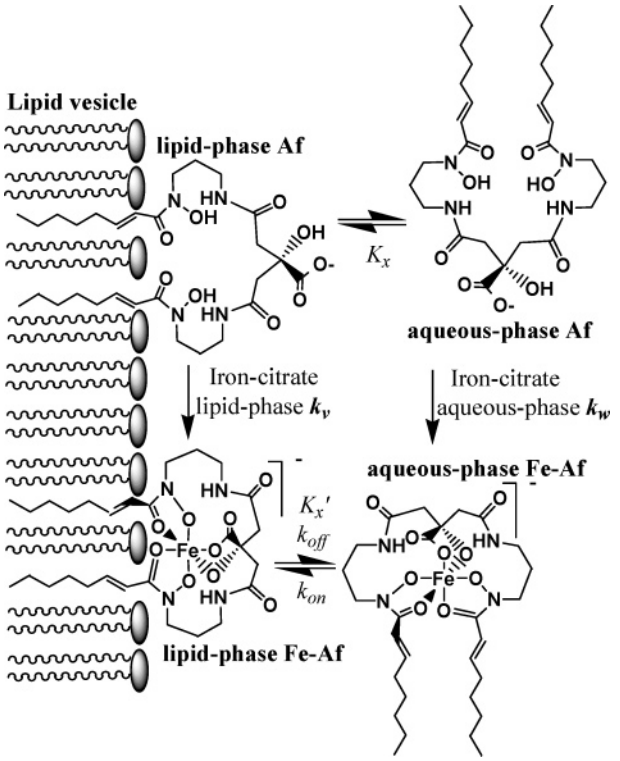

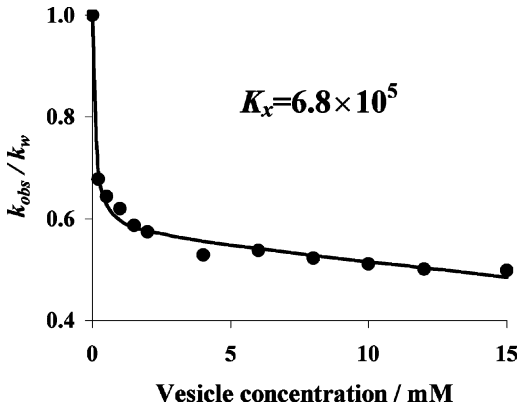

Figure 2. Lipid-concentration-dependent kinetics of iron acquisition mediated by **Af** and measurement for the lipid/aqueous phase partition coefficient of **Af**. The variation of relative iron-acquisition rates, k_{obs}/k_w, was measured over a range of the concentrations of DMPC SUV (0−15 mM). All the experimental conditions, except varied lipid concentrations, are the same as described for the experiment in Figure 1. The relative iron-acquisition rate, k_{obs}/k_w, was calculated from k_{obs} and k_w values that were obtained as the corresponding k_{pm} in eq 1 by fitting the absorbance change at 430 nm. The relative iron-acquisition rate, k_{obs}/k_w, shows a hyperbolic relationship with the increased concentration of lipids. The solid line was obtained by fitting eq 2 to the experimental data with $K_x = 6.8 \times 10^5$ for the partition coefficient of **Af** and $\alpha = 0.57$ for k_v/k_w.

(37) Bates, G. W.; Billups, C.; Saltman, P. *J. Biol. Chem.* **1967**, *242*, 2810.

iron-acquisition rate, $k_v/k_w = 0.57$ (the value of α), and the partition coefficient of **Af**, $K_x = 6.8 \times 10^5$. The value of $k_v/k_w = 0.57$ suggests that lipid-phase **Af** is capable of acquiring iron at about half the rate of the corresponding aqueous process.

Membrane Partitioning of Fe−Af and Measurement of its Molar Fraction Partition Coefficients. The lipid- and aqueous-phase partition coefficient of Fe−**Af** was measured by utilizing the fluorescence quenching property of paramagnetic Fe−**Af**. Outer-leaflet-labeled fluorescent vesicles were made simply by mixing pre-prepared DMPC SUV with NBD-PC fluorescent probes (see the Experimental Section). Fluorescence quenching observed upon mixing Fe−**Af** with the outer-leaflet-NBD-PC-labeled DMPC SUV was consistent with the partitioning of Fe−**Af** into the DMPC SUV outer-leaflet. According to a static quenching model (Perrin Model, see Supporting Information),[38] the fluorescence intensity will be directly related to the concentration of lipid-phase quencher as described in eq 3,[39] in which Φ_q and Φ_0 are the fluorescence intensities prior to and after quenching, [vesicle] is the molar concentration of lipid vesicles, $[Q]_v$/[vesicle] is the molar ratio concentration of lipid-phase quencher, and k_{qv} is the quenching coefficient. In this case, quencher molecules instantaneously interact with excited fluorescent molecules within an active sphere, and there is no prerequisite to initially produce fluorescent molecule−quencher complexes.[38] Equation 4 could further be derived from eq 3 by replacing $[Q]_v$/[vesicle] with the molar ratio of total quencher to concentration of vesicles, $[Q]_t$/[vesicle], where K_x' is the molar fraction partition coefficient of quencher and [water] is the molar concentration of water. The values of $\ln(\Phi_q/\Phi_0)$, the relative fluorescence intensities, were shown to be linear with the concentrations of Fe−**Af** ($[Q]_t$), indicating a good agreement with the Perrin Model described above (Figure S4 in the Supporting Information).

$$\frac{\phi_q}{\phi_0} = \exp\left(-k_{qv}\frac{[Q]_v}{[\text{vesicle}]}\right) \quad (3)$$

$$\ln\left(\frac{\phi_0}{\phi_q}\right) = \frac{k_{qv} \times K_x' \times [Q]_t}{K_x' \times [\text{vesicle}] + [\text{water}]} \quad (4)$$

The molar fraction partition coefficient, K_x', for Fe−**Af** in DMPC SUV at 20 °C and pH = 7.4 was obtained by fitting eq 4 with the relative fluorescence intensities, $\ln(\Phi_q/\Phi_0)$ (as described above and in the Experimental Section), of various concentrations of DMPC SUV (the ratio of total Fe−**Af** to DMPC is kept as a constant of 1:90). The experimental data and the resulting fit are shown in Figure 3 with $K_x' = 1.3 \times 10^4$, in which [vesicle]/$[Q]_t = 90$ and [water] = 55.6 M are used. In eq 4, fluorescence quenching arising from aqueous-phase Fe−**Af** and the self-absorption of Fe−**Af** are neglected because these two perturbing factors do not make significant contributions to the quenching process. (See Figures S1 and S5 in the Supporting Information.)

Similarly, the molar fraction partition coefficients of Fe−**Af** in DMPC SUV and egg-PC LUV at 37 °C were also obtained by measuring relative fluorescence intensities, $\ln(\Phi_0/\Phi_q)$ (as described above and in the Experimental Section), in the presence of various concentrations of lipid vesicles and Fe−**Af** (the ratio of Fe−**Af** to lipid vesicles was kept constant) using stopped-flow spectrophotometry. The values $K_x' = 2.2 \times 10^4$ in DMPC SUV and $K_x' = 7.7 \times 10^4$ in egg-PC LUV at 37 °C by fitting eq 4 to the experimental data (Figure S6) are consistent with that obtained in Figure S4. Apparently, the small temperature shift from 20 to 37 °C only slightly changes the partition coefficient of Fe−**Af** in DMPC. The relatively larger partition coefficient for Fe−**Af** in egg-PC is consistent with the longer hydrocarbon chains of egg-PC lipid. The quenching coefficient in egg-PC for the set of experiments was also obtained here with $k_{qv} = 13.0$.

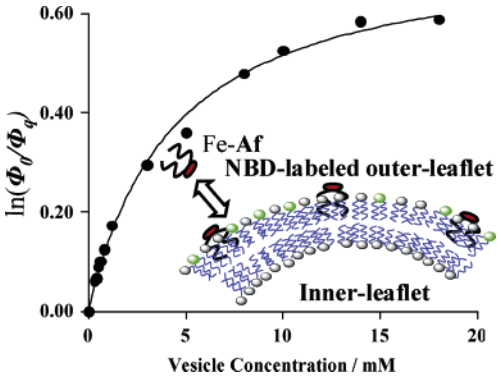

Figure 3. Measurement of the molar fraction partition coefficient for Fe−**Af** in DMPC SUV at 20 °C and pH = 7.4. Initial and quenched fluorescence spectra (λ_{exc} = 470 nm, λ_{em} = 540 nm) were recorded prior to and after the addition of Fe−**Af** into the solution of outer-leaflet-NBD-PC-labeled fluorescent vesicles. The molar ratio of Fe−**Af** to lipid vesicles, $[Q]_t$/[vesicle], was constant at 1:90, and the relative fluorescence intensities, $\ln(\Phi_0/\Phi_q)$, in the presence of various DMPC SUV concentrations (0.3−18 mM) were determined. The solid line shows the best fit of eq 4 to the experimental data with $K_x' = 1.3 \times 10^4$ for the partition coefficient of Fe−**Af** and $k_{qv} = 66.6$ for the quenching coefficient. Inset: cartoon description for this measurement.

Partitioning Rate and Dissociation Rate (k_{on}+k_{off}) for Fe−Af between DMPC Lipid and Aqueous Phase. The partitioning and dissociation of Fe−**Af** between aqueous/lipid phases were studied by utilizing the quenching property of paramagnetic Fe−**Af** on the double-leaflet-NBD-PC-labeled fluorescent DMPC SUV. Upon mixing Fe−**Af** with the NBD-PC-labeled fluorescent DMPC SUV at 37 °C, there was an extremely rapid quenching of fluorescence intensities that reached its equilibrium within the first second, followed by a slow decay of fluorescence with the half-life time around 10 min (for the latter, see the results for the flip-flop of Fe−**Af**). We interpreted the former as the partitioning of aqueous-phase Fe−**Af** into the outer-leaflet of lipid vesicles. By tracking the variation in fluorescence intensities versus time, we obtained the first-order decay constants (k_{dec}) of fluorescence intensity within the first second upon mixing by fitting eq 5 to the experimental data (vesicle concentration = 92−920 μM), in which Φ_t is the fluorescence intensity versus the time t, Φ_0 is the initial fluorescence intensity, Φ_∞ is the fluorescence intensity after reaching the partitioning equilibrium (normally within 1 s), and k_{dec} is the observed first-order rate constant of the fluorescent decay within the first second upon mixing with Fe−**Af**. Consequently, the partitioning rate, k_{on}, and the dissociation rate, k_{off}, are derived on the basis of eq 6, in which [vesicle] is the concentration of lipid vesicles. The correlation between various k_{dec} and corresponding vesicle concentrations is shown in Figure 4 with $k_{off} = 29\ s^{-1}$ for the dissociation rate of Fe−**Af** from the outer leaflet of lipid vesicles

(38) Birks, J. B. *Photophysics of Aromatic Molecules*; Wiley-Interscience: London, New York, Sydney, 1970.
(39) Weizman, H.; Ardon, O.; Mester, B.; Libman, J.; Dwir, O.; Hadar, Y.; Chen, Y.; Shanzer, A. *J. Am. Chem. Soc.* **1996**, *118*, 12368−12375.

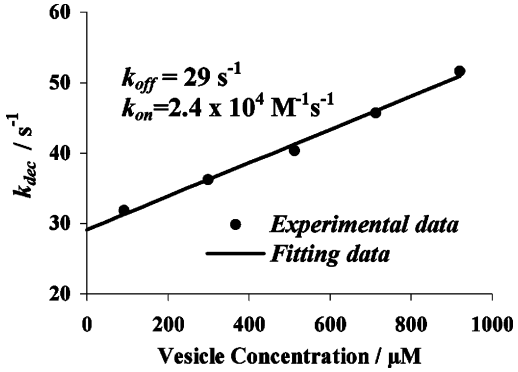

Figure 4. Measurements of the partitioning rate, k_{on}, and the dissociation rate, k_{off}, of Fe−**Af** between aqueous/lipid phases. The concentration of Fe−**Af** was kept constant (200 μM), and the concentration of NBD-PC-labeled fluorescent DMPC SUV was gradually varied from 92 to 920 μM. The first-order decay rate constants, k_{dec} (solid dots), were determined using eq 5 by fitting the changes of fluorescence intensities vs time upon mixing Fe−**Af** with the fluorescent-probe-labeled vesicles. The linear correlation between the first-order decay rate constants of fluorescence intensity vs lipid concentrations was followed. The solid line was obtained by fitting eq 6 to the rate constants with the intercept, $k_{off} = 29\ s^{-1}$, for the dissociation rate from the lipid phase and the slope, $k_{on} = 2.4 \times 10^4\ M^{-1}\ s^{-1}$, for the lipid-phase partitioning rate. The molar fraction partition coefficient of Fe−**Af** ($K_x' = 4.5 \times 10^4$) is derived from the values of k_{off} and k_{on} by the equation (k_{on}/k_{off})[water].

and $k_{on} = 2.4 \times 10^4\ M^{-1}\ s^{-1}$ for the partitioning rate of Fe−**Af** into the outer leaflet of lipid vesicles. These rates for Fe−**Af** are very consistent with those of other amphiphilic molecules.[40] In addition, the molar fraction partition coefficient, $K_x' = 4.5 \times 10^4$, is derived from the values of k_{off} and k_{on} by the equation (k_{on}/k_{off})[water], in which [water] = 55.6 M. This kinetically derived partition coefficient, $K_x' = 4.5 \times 10^4$, is in good agreement with the value of $K_x' = 2.2 \times 10^4$ (Figure S6) obtained via the equilibrium fluorescence quenching.

$$\ln \phi_t = \ln(\phi_\infty/\phi_0) \times (1 - \exp(-k_{dec} \times t)) + \ln \phi_0 \quad (5)$$

$$k_{dec} = k_{on} \times [\text{vesicle}] + k_{off} \quad (6)$$

Trans-Membrane Diffusion (Flip-Flop) of Fe−Af through Bilayers of Egg-PC LUV. To study the flip-flop kinetics of Fe−**Af** through lipid bilayers, we first made *inner-leaflet*-NBD-PC-labeled fluorescent egg-PC LUV, whose fluorescence intensities could be quenched only when extra-vesicularly added Fe−**Af** translocates to the inner-leaflet of the egg-PC LUV (see the Supporting Information and Figure S5). As described in the Experimental Section, stable inner-leaflet-NBD-PC-labeled fluorescent egg-PC LUVs were prepared from double-leaflet-labeled fluorescent egg-PC LUV by $Na_2S_2O_4$-mediated reduction of the outer-leaflet NBD probes and dioxygen bubbling to remove excess $Na_2S_2O_4$. Upon mixing Fe−**Af** with inner-leaflet-labeled fluorescent egg-PC LUV, we observed a decay of fluorescence. This decay was interpreted as the consequence from the translocation of Fe−**Af** through the bilayer membranes of the egg-PC LUV. The relationship between the flip-flop rate of Fe−**Af**, k_p, and the initial decay rate of relative fluorescence intensities, $\partial[\ln(\Phi_0/\Phi_{\Delta t})]/\partial t$, is shown in eqs 7 and 8.[42] A lipid-membrane flip-flop rate for Fe−**Af**, $k_p = 1.2 \times 10^{-3}\ s^{-1}$, and the molar fraction partition coefficient, $K_x' = 4.5 \times 10^4$, were obtained upon fitting eq 8 with the measured initial decay rates of relative fluorescence intensities, $\partial[\ln(\Phi_0/\Phi_{\Delta t})]/\partial t$, in the presence of various concentrations of egg-PC LUV (0−8 mM, the molar ratio of the total Fe−**Af** to egg-PC LUV was kept as a constant, 1:100). The partition coefficient obtained by this technique, $K_x' = 4.5 \times 10^4$, also showed a good agreement with the value of $K_x' = 7.7 \times 10^4$ (Figure S6) obtained via the equilibrium fluorescence quenching. A half-life time of 6×10^2 s of the flip-flop process for Fe−**Af** through the lipid membrane of egg-PC LUV could be deduced from the flip-flop rate of Fe−**Af**, $k_p = 1.2 \times 10^{-3}\ s^{-1}$.

In eq 7, aqueous-phase Fe−**Af** and outer-leaflet Fe−**Af** do not contribute to the time-dependent fluorescent decay using inner-leaflet-labeled fluorescent egg-PC LUV, due to the large distance (40 Å) between the inner and outer leaflet surfaces (see the control experiments for Figures S1 and S5 in the Supporting Information).[41] Distances between the fluorescent probe and quencher larger than 15 Å are ineffective for quenching.[38] The possibility for flip-flop of the NBD-PC fluorescent probes could be ignored in the present study because the flip-flop rate of phospholipids is intrinsically slow, with a half-life time more than 10 days in the absence of active lipid translocases.[43] In addition, we did not observe any bleaching of the fluorescence during the experiment upon mixing fluorescent-labeled egg-PC LUV with blank buffer.

$$\frac{\partial[\ln(\Phi_0/\Phi_{\Delta t})]}{\partial t} = \frac{k_{qv}}{[\text{vesicle}]} \times \frac{\partial[\text{Fe}-\mathbf{Af}]_{inner}}{\partial t} = k_p \times k_{qv} \times [\text{Fe}-\mathbf{Af}]_{outer} \quad (7)$$

$$\frac{\partial[\ln(\Phi_0/\Phi_{\Delta t})]}{\partial t} = k_{qv} \times k_p \times \frac{K_x' \times [\text{Fe}-\mathbf{Af}]_t}{K_x' \times [\text{vesicle}] + [\text{water}]} \quad (8)$$

Determination of Trans-Membrane Kinetics of Fe−Af using Proton NMR Spectroscopy. Partitioning and flip-flop of Fe−**Af** were also investigated using ^{1}H NMR spectroscopy by observing the evolution of the two proton resonances of the DMPC SUV choline *N*-methyl groups at 3.32 (outer leaflet) and 3.27 ppm (inner leaflet), which can be broadened upon treating with paramagnetic molecules, such as Fe−**Af**. It has been reported that only lipid-phase line-broadening reagents, rather than those in aqueous phase, are responsible for the signal change of the choline *N*-methyl groups of DMPC SUV.[14] For Fe−**Af** (Figure 6), a rapid broadening of the proton signals of the outer-leaflet *N*-methyl groups was observed within the initial 2 min upon the addition of 125 μM paramagnetic Fe−**Af** into 25 mM DMPC vesicles. This observation is consistent with the rapid partitioning of Fe−**Af** into the outer leaflets of DMPC

(40) Nichols, J. W.; Pagano, R. E. *Biophys. J.* **1981**, *33*, A117.

(41) Huang, C.; Mason, J. T. *Proc. Natl. Acad. Sci. U.S.A.* **1978**, *75*, 308−310.

(42) Equation 4 shows the relationship between the relative fluorescence intensity, $\ln(\Phi_q/\Phi_0)$, and the concentration of lipid-phase Fe−**Af**. Consequently, for the inner-leaflet-labeled fluorescent egg-PC LUV, the initial increase of inner-leaflet Fe−**Af** vs time upon mixing at 37 °C, $\partial[\text{Fe}-\text{Af}]_{inner}/\partial t$, could be deduced from the derivative of the relative fluorescence intensity vs time, $\partial[\ln(\Phi_0/\Phi_{\Delta t})]/\partial t$. This relationship is indicated in eq 7, in which $[\text{Fe}-\mathbf{Af}]_{inner}$ and $[\text{Fe}-\mathbf{Af}]_{outer}$ are the concentrations of inner-leaflet and outer-leaflet Fe−**Af**, respectively; the initial value of $[\text{Fe}-\mathbf{Af}]_{inner}$ is zero, and the initial value of $[\text{Fe}-\mathbf{Af}]_{outer}$ can be determined from the partitioning coefficient of Fe−**Af** (K_x') and the total concentration of the added Fe−**Af** and lipid vesicles; k_p is the flip-flop rate through bilayers of egg-PC LUV; [vesicle] is the concentration of egg-PC LUV. Equation 8 was derived from eq 7 with $k_{qv} = 13.0$, which was obtained from the data in Figure S6, K_x' for the molar fraction partition coefficient and $[\text{Fe}-\mathbf{Af}]_t$ for the total concentration of added Fe−**Af**.

(43) (a) Rothman, J. E.; Dawidowicz, E. A. *Biochemistry* **1975**, *14*, 2809−2816. (b) Roseman, M.; Litman, B. J.; Thompson, T. E. *Biochemistry* **1975**, *14*, 4826−4830.

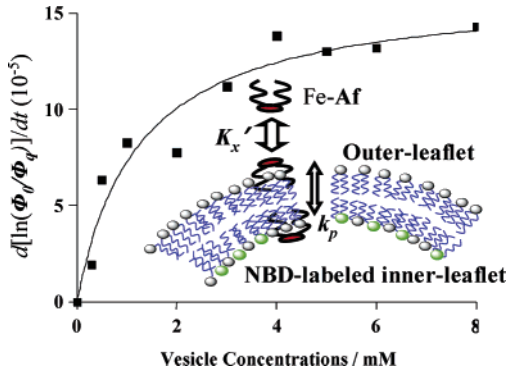

Figure 5. Rate measurement for the trans-membrane flip-flop of Fe−**Af** through egg-PC LUV. The changes in relative fluorescence intensity, $\ln(\Phi_0/\Phi_q)$, vs time, *t*, upon mixing Fe−**Af** (at 37 °C) with inner-leaflet-NBD-PC-labeled egg-PC LUV were recorded after a 10 s pre-equilibrium of Fe−**Af** between the aqueous phase and the outer leaflet of lipid vesicles. Φ_0 is the initial fluorescence intensity, and Φ_q is the quenched fluorescence intensity vs time, *t*. The molar ratio, $[\text{Fe}-\mathbf{Af}]_t/[\text{vesicle}]$, was constant at 1:100, and the changes of relative fluorescence intensities, $\ln(\Phi_0/\Phi_q)$, vs time *t* were recorded in the presence of various concentrations of inner-leaflet-NBD-PC-labeled egg-PC LUV(0−8 mM). The initial rate of the variation of the relative fluorescence intensities vs time, $\partial[\ln(\Phi_0/\Phi_{\Delta t})]/\partial t$, was obtained by measuring the slope of the initial change of the relative fluorescence intensities. The solid line is the best fit for eq 8 with $k_p = 1.2 \times 10^{-3}\ s^{-1}$ and $K_x' = 4.5 \times 10^4$, in which [vesicle] is the concentration of egg-PC LUV. Inset: cartoon description for this measurement.

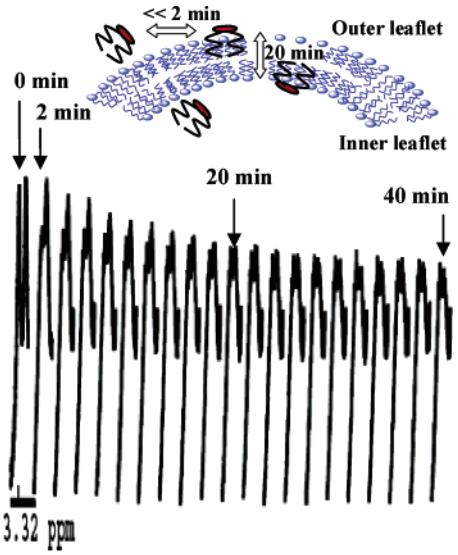

Figure 6. Lipid partitioning and trans-membrane flip-flop of Fe−**Af** using ^{1}H NMR line-broadening techniques. Fe−**Af** (125 μM) (the final concentration) was injected into an NMR tube containing 25 mM DMPC SUV at 20 °C. The proton resonances of the choline methyl groups of DMPC SUV were monitored with an interval of 2 min over a 40 min time scale. The upfield signal (3.28 ppm) and downfield signal (3.32 ppm) correspond to the inner-layer and outer-layer choline methyl groups of DMPC SUV, respectively. The broadening of the downfield methyl signals within the first 2 min is consistent with the initial rapid partitioning of Fe−**Af** into the lipid outer leaflet, while the slow broadening of the upfield methyl signals corresponds to the following trans-membrane flip-flop of Fe−**Af** through DMPC bilayer. The time for the equilibration of the latter process is within a 10 min scale. Inset: cartoon description for this measurement.

SUV. Subsequently, the proton signals of the inner-leaflet *N*-methyl groups broadened continuously. This relatively slow process was interpreted as the translocation of Fe−**Af** through DMPC SUV bilayers. Disruption of DMPC SUV in this case can be ruled out because the two proton resonances of the *N*-methyl groups were still well resolved and there was no significant change for the outer-leaflet signals during this later flip-flop. The rate of Fe−**Af** translocation through DMPC SUV bilayers can be estimated to be within a several-minute scale, which shows a good agreement with $k_p = 1.2 \times 10^{-3}\ s^{-1}$ (Figure 5) obtained for the flip-flop of Fe−**Af** through egg-PC LUV bilayers via the fluorescence quenching experiments. We also investigated the flip-flop property of Fe−**Af** using cholesterol-rich vesicles (egg-PC:cholesterol = 1:0.8). Only the ^{1}H NMR peaks of the outer-leaflet choline *N*-methyl groups were broadened within less than 2 min (similar as those shown in Figure 6), and the inner-leaflet choline *N*-methyl ^{1}H NMR peaks showed no change within at least 2 h. This observation suggests that the trans-membrane process of Fe−**Af** is inhibited under this condition, consistent with the flip-flop inhibitory effect of cholesterol reported before.[73]

To further assess the partitioning and trans-membrane processes of Fe−**Af**, the relaxation time T_1 of DMCP SUV choline *N*-methyl groups was measured, which is expected to dramatically decrease when the examined nuclei are close to paramagnetic molecules, such as Fe−**Af**.[44] As indicated in Figure 7, there was a rapid decrease of the relaxation time of DMPC SUV outer-leaflet *N*-methyl signals followed by a slow decrease of the relaxation time of its inner-leaflet *N*-methyl signals upon the treatment of 40 μM Fe−**Af** to 10 mM DMPC SUV. This observation is consistent with the rapid partitioning of Fe−**Af** into DMPC SUV outer leaflets and the subsequent relatively slow flip-flop through DMPC SUV bilayer membrane. A 10 min scale of the translocation process observed in Figure 7 is also in a good agreement with those obtained from the fluorescence quenching experiment and the ^{1}H NMR broadening experiment described above (Figures 5 and 6). In these different approaches employed to measure the membrane-translocation

(44) Wilkins, R. G. *The Study of Kinetics and Mechanism of Reactions of Transition Metal Complexes*; Allyn and Bacon, Inc.: Boston, 1974.
(45) Roberts G. *Langmuir−Blodgett Films*; Plenum Press: New York, 1990.
(46) Epand, R. M. *Biopolymers* **1997**, *43*, 15−24.
(47) Tsao, H. K.; Tseng, W. L. *J. Chem. Phys.* **2001**, *115*, 8125−8132.
(48) Hoyrup, P.; Davidsen, J.; Jorgensen, K. *J. Phys. Chem. B* **2001**, *105*, 2649−2657.
(49) Tanford, C. *The Hydrophobic Effect: Formation of Micelles and Biological Membranes*; John Wiley & Sons: New York, 1980.
(50) Peitzsch, R. M.; McLaughlin, S. *Biochemistry* **1993**, *32*, 10436−10443.
(51) Silvius, J. R.; Lheureux, F. *Biochemistry* **1994**, *33*, 3014−3022.
(52) Heerklotz, H.; Seelig, J. *Biophys. J.* **2000**, *78*, 2435−2440.
(53) Nichols, J. W.; Pagano, R. E. *Biochemistry* **1981**, *20*, 2783−2789.
(54) Ghomashchi, F.; Zhang, X. H.; Liu, L.; Gelb, M. H. *Biochemistry* **1995**, *34*, 11910−11918.
(55) Shahinian, S.; Silvius, J. R. *Biochemistry* **1995**, *34*, 3813−3822.
(56) Horwitz, L. D.; Sherman, N. A.; Kong, Y. N.; Pike, A. W.; Gobin, J.; Fennessey, P. V.; Horwitz, M. A. *Proc. Natl. Acad. Sci. U.S.A.* **1998**, *95*, 5263−5268.
(57) Pahl, P. M. B.; Yan, X. D.; Hodges, Y. K.; Rosenthal, E. A.; Horwitz, M. A.; Horwitz, L. D. *J. Biol. Chem.* **2000**, *275*, 17821−17826.
(58) Moss, R. A.; Bhattacharya, S. *J. Am. Chem. Soc.* **1995**, *117*, 8688−8689.
(59) Fattal, E.; Nir, S.; Parente, R. A.; Szoka, F. C. *Biochemistry* **1994**, *33*, 6721−6731.
(60) Daleke, D. L.; Huestis, W. H. *Biochemistry* **1985**, *24*, 5406−5416.
(61) Seigneuret, M.; Devaux, P. F. P. *Natl. Acad. Sci.* **1984**, *81*, 3751−3755.
(62) Lambert, T. N.; Boon, J. M.; Smith, B. D.; Perez-Payan, M. N.; Davis, A. P. *J. Am. Chem. Soc.* **2002**, *124*, 5276−5277.
(63) Boon, J. M.; Shukla, R.; Smith, B. D.; Licini, G.; Scrimin, P. *Chem. Commun.* **2002**, 260−261.
(64) Boon, J. M.; Smith, B. D. *J. Am. Chem. Soc.* **1999**, *121*, 11924−11925.
(65) Boon, J. M.; Smith, B. D. *J. Am. Chem. Soc.* **2001**, *123*, 6221−6226.
(66) Boon, J. M.; Smith, B. D. *Biophys. J.* **2001**, *80*, 2443.
(67) Shimojo, T.; Ohnishi, T. *J. Biochem.* **1967**, *61*, 89.
(68) Parish, C. A.; Rando, R. R. *Biochemistry* **1996**, *35*, 8473−8477.
(69) McLaughlin, S.; Aderem, A. *Trends Biochem. Sci.* **1995**, *20*, 272−276.
(70) Wedegaertner, P. B.; Wilson, P. T.; Bourne, H. R. *J. Biol. Chem.* **1995**, *270*, 503−506.
(71) Ratledge, C.; Dover, L. G. *Annu. Rev. Microbiol.* **2000**, *54*, 881−941.
(72) Dutzler, R.; Campbell, E. B.; Cadene, M.; Chait, B. T.; MacKinnon, R. *Nature* **2002**, *415*, 287−294.
(73) Kol, M. A.; van Laak, A. N. C.; Rijkers, D. T. S.; Killian, J. A.; de Kroon, A.; de Kruijff, B. *Biochemistry* **2003**, *42*, 231−237.

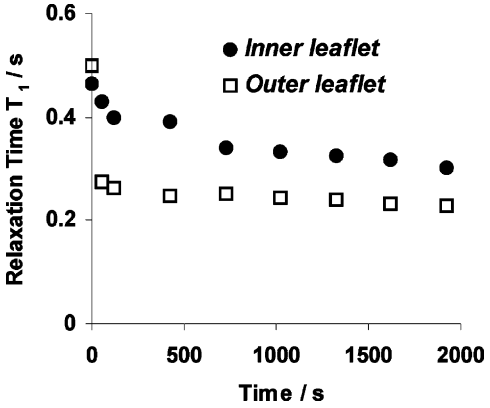

Figure 7. Membrane partitioning and trans-membrane flip-flop of Fe−**Af** monitored by the time-dependent variation of relaxation time T_1. Upon the addition of 40 μM Fe−**Af** into 10 mM DMPC SUV, the relaxation time of the upfield signal (3.27 ppm) for inner choline methyl groups and the downfield signal (3.32 ppm) for outer choline methyl groups was measured according to the method described in the Experimental Section. The initial decrease of the relaxation time for the outer choline methyl groups of DMPC SUV corresponds to the rapid partitioning of Fe−**Af** into the outer leaflet of lipid bilayers. The subsequent decrease of the relaxation time for inner choline methyl groups features the flip-flop of Fe−**Af** through the lipid bilayers of DMPC SUV. The latter process could reach the plateau regime within 10 min after the initial injection of Fe−**Af**.

process of Fe−**Af**, all consistently show that the translocation of Fe−**Af** through lipid bilayers is an efficient process with a time scale of about 10 min.

Measurements of Mean Molecular Areas (Mma) of Af and Af12 (its C-12 Analogue). The mean molecular areas (Mma) of amphiphilic molecules obtained by Langmuir−Blodgett techniques can help one to understand the conformations and orientations of these molecules at the aqueous/lipid interface.[45] To measure the Mma of **Af** and acinetoferrin-12 (**Af12** as shown in Figure 1), Langmuir−Blodgett experiments were carried out, in which **Af** and **Af12** were incubated onto the interface between air and subphase buffer. As shown in Figure 8, **Af**, **Af12**, and their ferric complexes (Fe−**Af** and Fe−**Af12**) form well-behaved Langmuir monolayers at the air/buffer interface. Mma values were obtained, with 52 Å^2 for **Af**, 88 Å^2 for **Af12**, 114 Å^2 for Fe−**Af**, and 166 Å^2 for Fe−**Af12**, by extrapolating the linear region of the plot in the usual way.[45] From Fe−**Af** to Fe−**Af12**, a significant Mma increase of 52 Å^2 was observed. A similar tendency was also shown from 52 Å^2 for **Af** to 88 Å^2 for **Af12**. Since **Af** and **Af12** have the same hydrophilic headgroups, the enhanced length of the hydrocarbon chains from **Af** to **Af12** would increase their Mma only if the two hydrocarbon chains of **Af** and **Af12** were not oriented parallel to each other at the air/buffer interface.[35,45] The smaller Mma of **Af** (both **Af** and Fe−**Af**) compared with those of the corresponding analogues (**Af12** and Fe−**Af12**) suggests this nonparallel orientation for the two hydrocarbon chains of both **Af** and **Af12** (Figures 9 and 10).[35] There is a larger Mma difference of 52 Å^2 between Fe−**Af** and Fe−**Af12** compared with that of 36 Å^2 between **Af** and **Af12**. This observation is consistent with our recent structural determination of Ga−**Af**, indicating that the two hydrocarbon chains of Fe−**Af** and Fe−**Af12** would have a more extended orientation with an angle around 130° than those of **Af** and **Af12** with an angle around 30° (Figure 9).[35] This different orientation of the two hydrophobic chains between **Af**(**Af12**) and Fe−**Af**(**Af12**) could partially account for the dramatic increase of Mma from apo to ferric species (62 Å^2

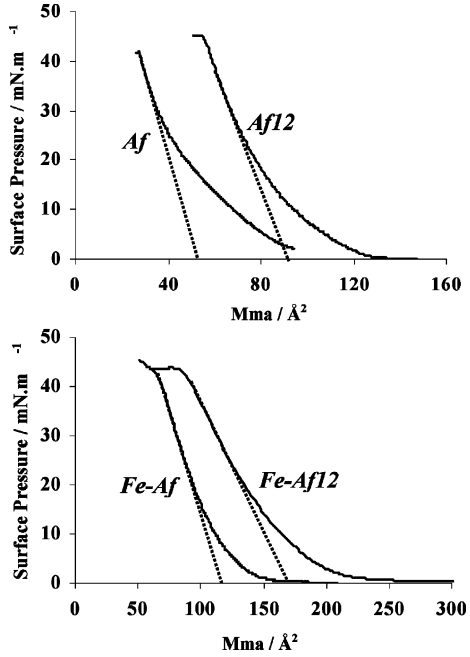

Figure 8. Measurements of mean molecular areas (Mma) using Langmuir−Blodgett techniques. As described in the Experimental Section, using Tris buffer as the subphase (pH = 8.0, 0.1 M KCl, 1 mM $CaCl_2$), Mma values of amphiphilic siderophores (**Af**, Af**12**, Fe−**Af**, and Fe−**Af12**) were obtained by extrapolating the linear region of surface pressure to the value of zero (52 Å^2 for **Af**, 88 Å^2 for Af**12**, 114 Å^2 for Fe−**Af**, and 166 Å^2 for Fe−**Af12**).

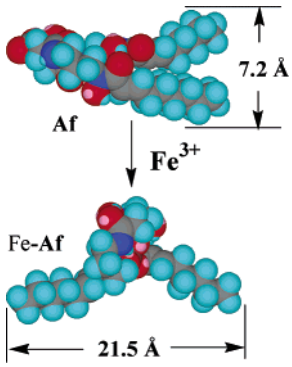

Figure 9. Phospholipid-like conformation of **Af** and the more extended conformation of Fe−**Af**. The optimized structures of **Af** and Fe−**Af** are reproduced from our recent studies.[35] Notice the significant conformational change of the two hydrocarbon chains of **Af** upon iron binding. The distance between the two terminal carbons is 7.2 Å, while this distance is increased to 21.5 Å upon iron binding. The color codes are defined as: C, gray; H, cyan; O, red; N, blue; Fe, brown.

between **Af** and Fe−**Af** and 78 Å^2 between **Af12** and Fe−**Af12**), the rest of which probably are due to the conformational change of the hydrophilic component of **Af** and **Af12**.

Discussion

Experimental Design. In the present paper, the membrane partitioning and trans-membrane flip-flop of Fe−**Af** are unambiguously discerned upon observing paramagnetic Fe−**Af**-mediated quenching of *outer*-leaflet-NBD-PC-labeled and *inner*-leaflet-NBD-PC-labeled fluorescent vesicles. The ^{1}H NMR line-broadening technique used here is another convenient approach to investigate these membrane processes. The improved protocol to prepare more *stable* inner-leaflet-NBD-PC-labeled fluorescent vesicles features the additional step for dioxygen-bubbling to

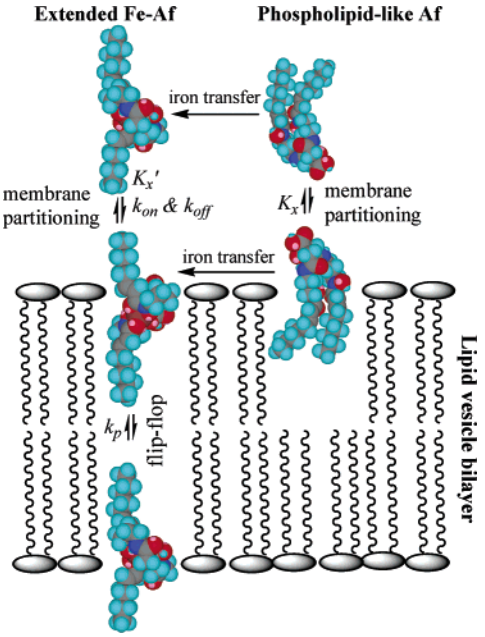

Figure 10. Schematic description of the iron-acquisition, membrane partitioning and trans-membrane flip-flop of acinetoferrin (**Af**). The 3D structures of **Af** and Fe−**Af** are reproduced from the previous studies, as shown in Figure 9.[35] The color codes are defined as: C, gray; H, cyan; O, red; N, blue; Fe, brown. K_x and K_x' are the molar fraction partition coefficients of **Af** and Fe−**Af**, respectively. The k_{on} and k_{off} terms are the partitioning and dissociation rates of Fe−**Af** between aqueous/lipid phases. The k_p is the rate of the trans-membrane flip-flop for Fe−**Af**. K_x, K_x', k_{on}, k_{off}, and k_p were all determined in this work with $K_x = 6.8 \times 10^5$, $K_x' = 2.2 \times 10^4$, $k_{on} = 2.4 \times 10^4$ M^{-1} s^{-1}, $k_{off} = 29$ s^{-1}, and $k_p = 1.2 \times 10^{-3}$ s^{-1}.

remove excess $Na_2S_2O_4$. All the designs described here are readily applicable to the study of membrane behavior of other paramagnetic amphiphiles.

Membrane Affinity of Af and Fe−Af. The partitioning of amphiphilic molecules between membrane and aqueous phase can play an important role in their biological functions through facilitating their interactions with specific binding sites on membrane surfaces or varying physical properties of the bound membranes.[46] Acinetoferrin (**Af**), with two equivalent *trans*-2-octenoyl chains, displays a considerable membrane affinity with the mole-fraction partition coefficient, $K_x = 6.8 \times 10^5$ (Figure 2), which is about 100-fold larger than those of ionic surfactants, such as sodium dodecyl 4-benzene sulfonate (SDS) and dodecyl pyridinium chloride (DPC).[47] The magnitude of the partition coefficient of **Af** falls into the range ($K_x = 10^5$−10^6) of the partition coefficients of lysolipids and fatty acids with a single C_{14}−C_{16} alkyl chain.[48] Given that **Af** has two symmetric hydrocarbon chains totaling 16 carbons (14 carbons if the two conjugated carbonyl groups are excluded), the consistent partition coefficients among **Af**, C_{14}−C_{16} lysolipids, and C_{14}−C_{16} fatty acids suggest that only the two hydrophobic chains of **Af** contribute to the lipid-membrane partitioning (a classical hydrophobic effect).[49,50] While the two *trans*-2-octenoyl chains of **Af** are separated from each other by a 15-atom linker, flexible adjustments of the hydrophilic linker apparently allow **Af** to adopt a relaxed conformation with a phospholipid-like structural motif (Figure 9).[35] Given that the free energies of partitioning into the lipid phase are increased by 0.8 kcal/mol per number of carbons, a value for the classical entropy-driven hydrophobic effect,[48,50,51] the membrane affinity of the 2-*n*-octyl chain phospholipid (D8PC) can be estimated to be $K_x = 2 \times 10^5$ on the basis of the partition coefficient of the 2-*n*-heptyl chain phospholipid (D7PC), $K_x = 1.1 \times 10^4$.[52] The consistent partition coefficients between **Af** with $K_x = 6.8 \times 10^5$ and D8PC with $K_x = 2 \times 10^5$ further confirm a phospholipid-like structure for **Af** (Figure 9). The results in Figure 8 show that **Af12**, with longer hydrocarbon chains, has a Mma 36 Å^2 larger than that of **Af** (52 Å^2 for **Af** and 88 Å^2 for **Af12**). This observation indicates that the two hydrocarbon chains of **Af** and **Af12** are not exactly parallel. Nevertheless, the slight nonparallel arrangement of the hydrocarbon chains of **Af** does not significantly change its phospholipid-like membrane affinity.

As shown in Figure S6, the partition coefficient, K_x', of Fe−**Af** dramatically drops to 2.2×10^4 upon the formation of Fe−**Af** from **Af**. A 30-fold decrease of the partition coefficients from 6.8×10^5 for **Af** to 2.2×10^4 for Fe−**Af** corresponds to a loss of two or three methylene groups from the lipid-phase subunits of **Af**, if lipid-phase partitioning free energies of 0.8 kcal/mol per carbon are assumed.[48,50,51] This large change in membrane affinity is most remarkable since six *hydrophilic* oxygen functionalities become buried upon iron binding by **Af**.[35] We argue that this large change in the partition coefficients of **Af** and Fe−**Af** can be attributed to the change in the geometry of the hydrophilic headgroup and corresponding reorientation of two *trans*-2-octenoyl chains imposed upon chelating iron. We have recently shown that the most stable conformer of Fe−**Af** is the *N-cis-cis*-conformation,[25,35] in which the two hydrophobic chains are antiparallel with each other, as shown in Figure 9. The results based on Langmuir−Blodgett experiments (Figure 8) also support the more extended conformation of Fe−**Af** compared with that of **Af** by two lines of evidence: (i) the large 62 Å^2 increase of Mma from 52 Å^2 for **Af** to 114 Å^2 for Fe−**Af**; and (ii) another 52 Å^2 enhancement of Mma from 114 Å^2 of Fe−**Af** to 166 Å^2 of Fe−**Af12**. These results are consistent with the phospholipid-like orientation of **Af** and the more extended conformation of Fe−**Af** (Figure 9). It is obvious that Fe−**Af** cannot adopt the orientation of classical amphiphilic molecules with all alkyl chains in a lipid phase and hydrophilic headgroups in an aqueous phase. Instead, the most optimal arrangement should adopt a maximal partitioning of both *trans*-2-octenoyl chains into the lipid phase, which probably accounts for the loss of its partitioning ability about two or three methylene groups as discussed above. Consequently, we assume that the more extended conformation of Fe−**Af** compared with the phospholipid-like structural motif of **Af** is the origin of the diminished membrane affinity of Fe−**Af**. This conformational rearrangement of the two lipophilic side chains upon iron binding has a larger effect on the lipid- and aqueous-phase partitioning than for octanol−water (30-fold decrease for the former vs 8-fold decrease[35] for the latter).

Dynamics of Lipid-Phase Partitioning and Trans-Membrane Flip-Flop of Fe−Af. The kinetic studies of the partitioning of Fe−**Af** into the outer leaflet of DMPC SUV (Figure 4) indicate that Fe−**Af** can rapidly diffuse into the lipid phase with the large partitioning rate, $k_{on} = 2.4 \times 10^4$ M^{-1} s^{-1}. On the other hand, the rate of the dissociation of Fe−**Af** from the lipid membrane is also very fast, with a dissociation rate of $k_{off} = 29$ s^{-1}.[14,40] The rapid equilibration of Fe−**Af** between lipid and aqueous phase can guarantee a homogeneous distribution of Fe−**Af** among the entire lipid population. For instance, the equili-

bration time for both lipid partitioning and dissociation can be narrowed into a 10 ms scale in the presence of 1 mM lipid vesicles. Fast partitioning and dissociation between lipid and aqueous phase have been observed for other amphiphilic molecules with moderate membrane affinities, such as some phospholipids[40,53] and lipoproteins.[51,54]

Kinetic studies showed that Fe−**Af**, a monoanion at neutral pH, translocates readily through membrane bilayers with a flip-flop rate of 1.2×10^{-3} s^{-1} and a half-life time around 10 min (Figure 5). These results are comparable with those obtained from the kinetic studies employing the techniques of paramagnetic-induced ^{1}H NMR line-broadening (Figure 6) and T_1 relaxation (Figure 7). Although it has been proposed that hydrophobic components of amphiphilic siderophores could facilitate the flip-flop through lipid membrane,[56,57] this is the first time that the flip-flop kinetics of ferric siderophores have been directly measured. The ready translocation of Fe−**Af** through membrane bilayers is different from what is observed for classical amphiphilic molecules, such as phospholipids, for which the flip-flop process is inherently slow with a typical half-life time of several days[43] and could only be promoted by natural or artificial translocases.[58−62] We assume that the facility of the flip-flop process of Fe−**Af** through lipid bilayers is due to the special extended conformation of Fe−**Af** (Figures 9 and 10). This extended conformation could facilitate the flip-flop process in at least three ways. First, most of the polar residues of **Af**, such as α-hydroxyl carboxylic acid and hydroxamic acids, are buried inside and coordinated to the central iron, while the portions of **Af** exposed to the outside mainly consist of the hydrocarbon skeleton. Such an arrangement with the polar components inside and the nonpolar components outside would largely benefit the lipo-solubility and, thereby, the flip-flop of Fe−**Af**. This principle has been applied to synthesize artificial phospholipid translocases, for which the key idea is to bury polar groups of phospholipids by designed translocases and thus accelerate the transverse diffusion of amphiphilic phospholipids.[62−66] Second, the negative charge of Fe−**Af** is redistributed among the ferric center and its six coordinating oxygens. This delocalization of the negative charge could further facilitate the flip-flop process. Third, as discussed in the previous section for the partition coefficient of Fe−**Af**, some portions of the hydrophobic chains of Fe−**Af** (two or three methylene groups) compared with that of **Af** are forced to be exposed to the aqueous phase rather than the lipid phase due to the constraint of the extended conformation of Fe−**Af**. In the process of a flip-flop, these methylene carbons will be buried in the lipid phase again and, thereby, gain the additional 2 kcal/mol free energy (0.8 kcal/mol per number of carbons).[48,50,51] This process can partially compensate for the free-energy cost of burying the polar residues of Fe−**Af** in the lipid phase. Therefore, we assume that the more extended conformation of Fe−**Af** in Figure 9 plays a significant role in both the membrane partitioning and trans-membrane flip-flop. This extended conformation is also responsible for Fe−**Af**-mediated vesicle disruption and fusion that we have reported recently.[35] Figure 10 depicts the process of membrane partitioning and trans-membrane flip-flop of Fe−**Af**.

On the basis of the current results for the translocation of Fe−**Af** through lipid bilayers, we notice that Fe−**Af** exhibits comparable abilities for flip-flop rates through either DMPC SUV membranes or egg-PC LUV membranes with a similar half-life time of 10 min (Figures 5−7). The mean molecular area (Mma) of the outer-leaflet lipid for SUV is about 74 Å^2 per lipid, while the value for the inner-leaflet lipid is only 61 Å^2 per lipid.[41] For LUV, Mma values of the inner-leaflet and outer-leaflet lipids are both around 66 Å^2.[67] Thus, Fe−**Af** with a Mma of 114 Å^2 (Figure 8) apparently is not sensitive to the small curvature difference of 8 Å^2 between SUV and LUV. The flip-flop inhibitory effect of cholesterol suggests that the trans-membrane ability of Fe−**Af** is sensitive to the membrane stiffening caused by cholesterol.

Comparison between Acinetoferrin and Marinobactin E. It is interesting to compare the properties of **Af** and marinobactin E (Figure S7) since both the siderophores (i) chelate iron(III) with two hydroxamic acids and one α-hydroxyl carbonyl subunits, (ii) process the net charge "−1" at neutral pH for both apo and ferric species, and (iii) include the total 16 carbons as their hydrophobic components. In contrast to the slow kinetics of the membrane dissociation/association of ferric marinobactin E ($k_{off} = 4.4 \times 10^{-3}$ s^{-1} and $k_{on} = 1.0$ M^{-1} s^{-1}, respectively),[14] Fe−**Af** shows rapid redistribution among bulk lipid components with the dissociation/partitioning rates of $k_{off} = 29$ s^{-1} and $k_{on} = 2.4 \times 10^4$ M^{-1} s^{-1}, respectively. The cause for the slower dissociation/partitioning rates of marinobacin E between the aqueous/lipid phase compared with those of Fe−**Af** and other amphiphilic molecules (e.g., $k_{on} = 4 \times 10^5$ M^{-1} s^{-1} for C_{12}−NBD-PC)[40,51,53,54] is not clear. **Af** and marinobactin E show remarkably similar partition coefficients despite their overall structural difference (**Af** in Figure 1 vs marinobactin E in Figure S7, $K_x = 6.8 \times 10^5$ for **Af** and $K_x' = 2.2 \times 10^4$ for Fe−**Af** in this work vs $K_x = 6.3 \times 10^5$ and $K_x' = 1.3 \times 10^4$ for marinobactin E and ferric marinobactin E).[14] Although the two siderophores show a large decrease of their membrane affinities upon iron binding, the origins for these decreases must be completely different from each other. As discussed in this work, we suggest that the decrease of the membrane affinity of **Af** upon binding iron is mainly due to the structural change of the two *trans*-2-octenoyl chains from phospholipid-like **Af** to more extended Fe−**Af**, whereas the decrease of the partition coefficients of marinobactin E upon binding iron must be related to the conformational change of the hydrophilic components of marinobactin E.[14] Upon iron binding, the Mma decreases from 79 Å^2 for marinobactin E to 56 Å^2 for its iron complex,[14b] while there is a remarkable increase of Mma from 52 Å^2 for **Af** to 114 Å^2 for Fe−**Af**. We have also shown that Fe−**Af** flip-flops readily through membranes, which was not observed for ferric marinobactin E. This observation suggests that it is the special properties of Fe−**Af** instead of its common anionic property or the positive potential of PC membranes[72] that account for the remarkable flip-flop rate of Fe−**Af** through PC membranes.

Biological Implications of Membrane Dynamics of Af and Fe−Af. Upon the invasion of hosts, pathogenic *Acinetobacter* pathogens start to synthesize **Af** that can either partition into the bacterial outer membranes or diffuse into host tissue. Consequently, a dynamic distribution of **Af** would occur between the medium and cellular lipid components. These amphiphilic siderophores might then access the host iron pools.[71] The anionic **Af** may translocate through host membranes because hydrophobic anions flip-flop relatively easily due to the positive electrostatic potential of the biological membranes.[72]

After iron chelation, Fe−**Af** would become *more* diffusive than **Af**, due to the ready membrane permeation, rapid equilibrium among all lipid components, and smaller partition coefficient of Fe−**Af**. The effect of moderate membrane affinity has been proposed to provide the facile redistribution of some lipopeptides among the cells.[46,69] The additional interactions between Fe−**Af** and outer-membrane receptors would facilitate the bacterial internalization of Fe−**Af**. It has been reported that such specific interactions with membrane-bound proteins significantly contribute to the lipid-phase-partitioning process of certain lipoproteins, such as MARCKS.[46,68,69] The membrane affinity of Fe−**Af** with $K_x' = 2.2 \times 10^4$ can be the initial driving force to concentrate Fe−**Af** from three-dimensional bulk solution into two-dimensional membrane surface. This initial recruiting can facilitate the subsequent receptor binding.[46,55,68,70]

Summary and Conclusions

Using *inner*- and *outer*-leaflet-labeled fluorescent vesicles and ^{1}H NMR line-broadening techniques, the membrane dynamics of a pathogenic siderophore, acinetoferrin (both **Af** and Fe−**Af**) were studied from a variety of aspects, including the membrane affinities of **Af** and Fe−**Af**, the trans-membrane permeability of Fe−**Af**, and its partitioning/dissociation between aqueous/lipid phases. Upon binding iron(III), the membrane affinity of **Af** decreases 30-fold. Fe−**Af** can rapidly partition and dissociate between aqueous/lipid phases with the large kinetic rate constants. The flip-flop process of Fe−**Af** is also fast, compared with other amphiphilic molecules. These observations are related to the more extended conformation of Fe−**Af** compared to that of **Af**. The remarkable similarities and differences between **Af** and marinobactin E are also discussed. As proposed in this work, one of the potential biological implications from these observations is that the physical properties of acinetoferrin produced by this pathogenic bacterium are tuned to access host iron pools and then transport iron to the invading bacterial pathogen.

Acknowledgment. The authors thank Dr. Istvan Pelczer and Dr. Carlos Pacheco for assistance with the NMR experiments, and Dr. Guofeng Xu for assistance with the lipid-vesicle preparation and the Langmuir−Blodgett experiments. Support of this work by the National Science Foundation (CHE-0221978) through the Environmental Molecular Science Institute (CEBIC) at Princeton University is gratefully acknowledged.

Supporting Information Available: Figures S1−S7 and their experimental descriptions. This material is available free of charge via the Internet at http://pubs.acs.org.

JA044230F